Fracture processes numerical modeling of elastic-brittle bodies with statistically distributed subregions strength values

E.V. Feklistova, A.I. Mugatarov, V.E. Wildemann
Center of Experimental Mechanics, Perm National Research Polytechnic University, Russia
cem.feklistova@mail.ru, https://orcid.org/0000-00020025-6204
cem_mugatarov@mail.ru, https://orcid.org/0000-0002-2229-8181
wildemann@pstu.ru, https://orcid.org/0000-0002-6240-4022

A.A. Agishev
The Engineering School of Information Technologies, Telecommunications and Control Systems, Ural Federal University, Russia
agishevanton1017@gmail.com, https://orcid.org/0009-0005-0067-4296

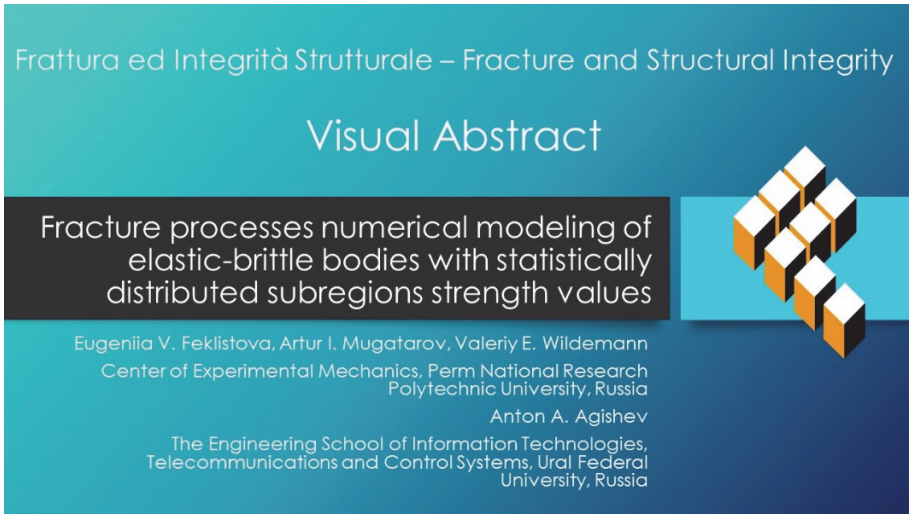

Citation: Feklisova, E.V, Mugatarov, A.I., Wildemann, V.E., Agishev, A.A., Fracture processes numerical modeling of elastic-brittle bodies with statistically distributed subregions strength values, Frattura ed Integrità Strutturale, 68 (2024) 325-339.

Received: 23.11.2023
Accepted: 29.02.2024
Published:: 05.03.2024
Issue: 04.2024

KEYWORDS. Fracture, Finite element method, Numerical modeling, Brittle body, Strength properties distribution.

INTRODUCTION

Providing the strength, reliability and safety of critical structures requires studying their mechanical behavior not only under standard conditions but also in case of microdefects nucleation and propagation [1, 2]. Numerical modeling is a broad approach encompassing a range of techniques and models, which uses computational methods and algorithms to simulate and analyze the mechanical behavior of materials under various conditions, including stress and fracture in the context of materials science and engineering [3-7]. There are many approaches (finite element method [8],

extended finite element method [9-10], extended virtual element method [11-12], peridynamics [13], finite element discretized symplectic method [14], meshfree method [15], etc.) and material behavior models (continuum damage models [16-17], cohesive crack models [18-20], bridged crack models [21], etc.) to simulate crack propagation and damage accumulation in solids.

One of the most widely used approaches is connected with finite element stiffness properties reduction if the failure criteria are fulfilled [3, 22-25]. This approach is one of the simplest, but requires taking into account several aspects. Firstly, the numerical procedure should be organized to take into account the possibility of failure criterion fulfillment simultaneously in different finite elements [26-28]. The second aspect is the selection of the loading step size [29-31]. The fixed step value must be small enough to describe the fracture process accurately, so the automatic step is more commonly used. Finally, the finite element mesh size has a great influence on the fracture modeling results [4, 25, 32-36]. Solving the convergence problem of an elastic solution may not be sufficient. All these aspects of elastic-brittle bodies fracture modeling were previously discussed by authors in [37].

Besides, the structural elements mechanical properties (most especially strength) statistical distribution over the body volume can also significantly affect the fracture process modeling results [23, 38-47]. This feature was widely discussed in problems of fibrous composites (consisting a large number of filaments with various strength properties [43, 46-47]) properties prediction [46, 48-49]. However, a small number of works investigate the damaging processes of elastic-brittle solids with stress concentrators taking into account the strength characteristics distribution, which may cause not only the load bearing capacity change, but the fracture mechanisms conversion.

This work is devoted to the fracture processes numerical modeling of elastic-brittle bodies with statistically distributed subregions strength values, focusing on the distribution range and stress concentration influence. The novel formulation of the boundary value problem of the elastic-brittle solid fracture and its solution algorithm are developed and given in the section below. The problem of the kinematic static loading of a plate (made of a model elastic-brittle material) with the stress concentrator is considered to prove the applicability of developed algorithm and to study the regularities of fracture process when the subregions' strength properties are statistically distributed. A number of numerical experiments are carried out; the results are presented and analyzed in the section «Results and discussion». The loading diagrams and corresponding graphs of the destroyed elements number for various uniform distribution range values are plotted. The kinetics of bodies damage accumulation processes are studied. The significant influence of the finite elements properties distribution and the stress concentration value on the fracture processes modeling results is noted. The final section closes the paper with the main conclusions of the work.

BOUNDARY VALUE PROBLEM AND ITS SOLUTION ALGORITHM

This section introduces the boundary value problem formulation. In order to take into account the strength properties' distribution, the solid can be represented as a set of N subregions, which material is homogeneous, isotropic and elastic-brittle. The elastic properties for each subregion are equal, but ultimate strength values σ_B are various. The inhomogeneity of ultimate strength values can be represented as follows:

$$\begin{cases} \chi^{(m)}(\bar{r}) = \begin{cases} 1, \bar{r} \in V_m \\ 0, \bar{r} \notin V_m \end{cases} \\ \sigma_B(\bar{r}) = \sum_{m=1}^{N} \sigma_B^{(m)} \chi^{(m)}(\bar{r}) \end{cases} \tag{1}$$

Here $\bar{r}$ is the radius vector; $\chi^{(m)}$ is the indicator function, characterizing the point location in the subregion indexed (m) with the volume V_m; V is the entire body volume; σ_B is the piecewise-constant function that specifies the ultimate strength values distribution over the solid.

We consider the fracture process, where failures of multiple subregions occur. Thus, the deformation process history must be taken into account. It can be implemented using the process parameter t (as a conditional analogue of time) introduced into the problem. Therefore, any stress, strain or displacement component should depend not only on the coordinates, but the process parameter too.

Since each subregion is elastic-brittle, we can assume that its destruction occurs when the maximum value of the first principal stress σ_1 in its area reaches the ultimate strength value (this hypothesis is applicable for the elastic-brittle materials).

However, each subregion has its own σ_B value. Hence, the overload factor K (defined as the ratio of σ_1 to σ_B) should be considered to allow comparison of the failure risk between various subregions of the solid:

$$K\left(\overline{r},t\right)=\frac{\sigma_1\left(\overline{r},t\right)}{\sigma_B\left(\overline{r}\right)} \tag{2}$$

The failure of any subregion leads to an almost instantaneous stress field change, which may cause the failure criterion fulfillment in many subregions at the same time. Following the traditional logic, we should destroy all of them on the next step. On the other hand, destruction of the most overloaded subregion may cause the unloading in the other one, where the failure criterion was previously fulfilled. Since this case seems to be more accurate and physical, we propose to destroy only one subregion with the highest overload factor value at each step, leading to more accurate damaging process description. Based on the foregoing, the integrity parameter of subregions, including the failure criterion, can be written as follows:

$$\begin{cases}\lambda^{(m)}\left(t\right)=\begin{cases}0,\exists\,\tau\le t:\max\limits_{V_m}\left(K\left(\overline{r},\tau\right)\right)=\max\limits_{V}\left(K\left(\overline{r},\tau\right)\right)\ge 1\\ 1,\nexists\,\tau\le t:\max\limits_{V_m}\left(K\left(\overline{r},\tau\right)\right)=\max\limits_{V}\left(K\left(\overline{r},\tau\right)\right)\ge 1\end{cases}\\ \lambda\left(\overline{r},t\right)=\sum\limits_{m=1}^{N}\lambda^{(m)}\left(t\right)\chi^{(m)}\left(\overline{r}\right)\end{cases} \tag{3}$$

Here $\lambda^{(m)}$ is the integrity parameter (the opposite of the damage parameter) of the subregion (m); t (or τ) is the conditional process parameter; λ is a piecewise-constant function, reflecting the integrity parameters' distribution over the solid.
To finish the boundary value problem formulation, we apply the equations of equilibrium (no mass forces are considered), the strain-displacement equations (since the strains in the destructed subregions can be large, the Lagrangian strain tensor is preferrable) and generalized Hooke's law, including the integrity parameter:

$$\begin{cases}\sigma_{ij,j}\left(\overline{r},t\right)=0\\ \varepsilon_{ij}\left(\overline{r},t\right)=\frac{1}{2}\left(u_{i,j}\left(\overline{r},t\right)+u_{j,i}\left(\overline{r},t\right)+u_{k,i}\left(\overline{r},t\right)u_{k,j}\left(\overline{r},t\right)\right)\\ \sigma_{ij}\left(\overline{r},t\right)=\lambda\left(\overline{r},t\right)C_{ijkl}\varepsilon_{kl}\left(\overline{r},t\right)\end{cases} \tag{4}$$

Here σ_{ij} is the stress tensor; ε_{ij} is the Lagrangian strain tensor; u_i is the displacement vector; C_{ijkl} is the elastic constants tensor. The problem (1)–(4) is supplemented by the boundary conditions:

$$\begin{cases}u_i\left(\overline{r},t\right)\big|_{\Gamma_u}=u_i^0\left(\overline{r},t\right)\\ \sigma_{ij}\left(\overline{r},t\right)n_j\left(\overline{r}\right)\big|_{\Gamma_S}=S_i^0\left(\overline{r},t\right)\end{cases} \tag{5}$$

where u_i^0 is the displacement applied to the boundary Γ_u; S_i^0 is the stress vector applied to the boundary Γ_S; n_j is the unit normal vector to the boundary Γ_S.
Several advantages of the proposed boundary value problems are noted. At first, the mechanical properties' statistical distribution over the body volume is taken into account. Therefore, this boundary value problem can be successfully applied in the problems of inhomogeneous structures (from concretes, fiber reinforced plastics, etc.) fracture using explicit material's structure modeling. Secondly, the destruction of only one most overloaded subregion and introduction of the process parameter t make the proposed boundary value problem more accurate and physical (unlike the problems where the failure criterion fulfillment leads to instant subregion's destruction). Thirdly, any failure criterion or their complex can be used in this boundary value problem by simple changing the Eqns. (2)–(3). However, some disadvantages are found out. Firstly, only the elasticity model is used (unlike, for example, the cohesive crack model, where the complete stress-strain curve of the material is applied). Secondly, other mechanical interactions (friction, etc.) near the damaged subregions are not taken

into account. Therefore, the proposed model has limited applicability in solving the problems where the interaction between the macrodefect surfaces (during compression or shear) occurs. Thus, the modification of the criterion (3) is necessary, it may be implemented using the complex of failure criteria. Nevertheless, noted disadvantages do not interfere the proposed boundary value problem application in fracture processes modeling of elastic-brittle bodies under tensile loadings.

The boundary value problem (1)–(5) can be solved numerically with the finite element method. In this case, each finite element (FE) can represent one subregion with individual strength properties. The following feature of the boundary value problem solution algorithm must be considered: the destruction of any FE leads to possible fulfillment of the failure criterion in the other FE. Therefore, the problem must be solved several times under similar boundary conditions until the steady state is achieved (no FE have to be destroyed). This nonequilibrium damage accumulation process appears on the calculated loading diagram in the form of the sharp load drop. This process may also lead to the complete solid's destruction (its division into several parts), so the critical value of the external load (denoted as P_{crit} and calculated as the sum of the reaction forces in each node of the body's boundary with applied displacement) should be selected to indicate the end of the fracture process.

Moreover, to describe the fracture process accurately, it is reasonable to use an automatically selected loading step (in comparison with the fixed step value). Since the body's material is linear-elastic, the following procedure can be implemented: if the failure criterion is not fulfilled in any FE, the u_i^0 and S_i^0 increase $1/K_{max}$ times, where K_{max} is the maximum overload ratio value over the solid. Otherwise, the boundary conditions remain the same, and FE damaging process continues.

Based on the foregoing, the boundary value problem (1)–(5) solution algorithm is:

1) Body's construction and meshing, generating FE ultimate strength values, entering material properties;
2) Boundary conditions creation, u_i^0 and S_i^0 values should be small to prevent the fracture criterion fulfillment anywhere;
3) Stress-strain state calculation;
4) Calculation of the external load value (ELV). If its value is less than P_{crit}, the fracture modeling process ends (except for the first step);
5) The overload ratio K field calculation, its maximum value K_{max} definition;
6) If $K_{max} \geq 1$, then destroy the most overloaded FE and go to step 3, else go to step 7;
7) Magnify the boundary conditions $1/K_{max}$ times, go to step 3.

The flow chart of the algorithm is presented in Fig. 1. The expediency of the proposed algorithm usage in comparison with differently organized was proved by authors in [32]. As a result of the boundary value problem solution, we obtain the loading diagrams and data on damage accumulation kinetics.

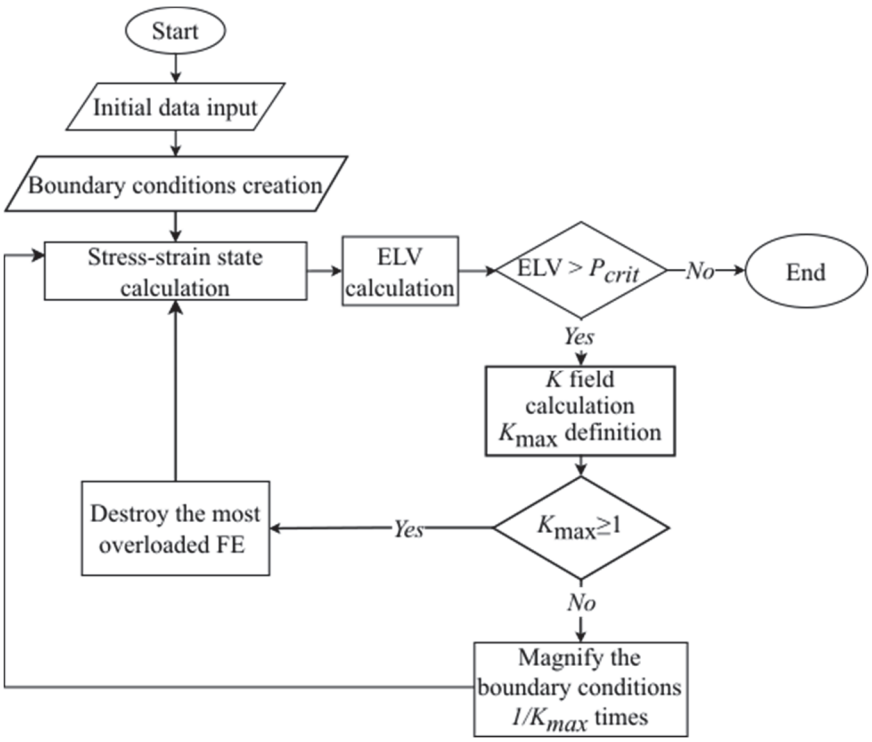

Figure 1: The flow chart of the boundary value problem solution algorithm

In order to investigate the applicability of proposed boundary value problem statement and the influence of the finite elements' strength properties distribution on the elastic-brittle bodies fracture processes, we consider the problem of kinematic static loading of a plate (100 mm wide, 20 mm height and 1 mm thick, plane stress state) with the stress concentrator in the shape of half ellipse (minor semiaxis 1 mm and major semiaxis h mm). The body's geometry is shown in the Fig. 2.

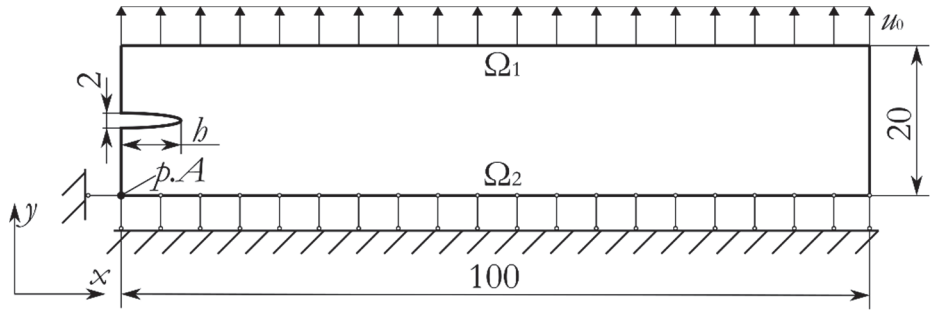

Figure 2: The geometry of solid with the stress concentrator and boundary conditions

The boundary conditions are:

$$\begin{cases} u_y(t)\big|_{\Omega_1} = u_0(t) \\ u_y(t)\big|_{\Omega_2} = 0 \\ u_x(t)\big|_{p.A} = 0 \end{cases} \tag{6}$$

Here Ω_1, Ω_2 are the top and bottom boundaries of the body; point A ($p.A$) is the lower left corner of the body, u_0 is the top boundary's displacement (Fig. 2).

In order to investigate the regularities of elastic-brittle bodies fracture taking into account the FE strength values distribution, we consider a model material without being tied to the real materials. The elastic properties of each FE are equal: Young's modulus E=210 GPa and Poisson's ratio ν=0.3. The ultimate strength values of FE are distributed by the uniform distribution within the minimum value of σ_{Bmin} and maximum value of σ_{Bmax}. In all the cases the average ultimate strength value is similar, $\sigma_{Bm}=0.5(\sigma_{Bmin}+\sigma_{Bmax})$=420 MPa. As is known, the standard deviation of uniform distribution is calculated as: $\delta=(\sigma_{Bmax}-\sigma_{Bmin})/(2\sqrt{3})$. On the other hand, it is more convenient to use the relative parameter $\alpha=\sqrt{3}\delta/\sigma_{Bm}$, $\alpha\in[0;1]$, which characterize the range of uniform distribution. The FE strength properties generation is carried out using Python pseudo random number generator as follows:

$$\sigma_B^{(m)} = \left((2x-1)\alpha+1\right)\sigma_{Bm} \tag{7}$$

Here (m) is the FE index, $m\in[1;N]$, x is the arbitrary number between 0 and 1, chosen by the uniform distribution. The α parameter is varied within [0;0.9] range with the increase step of 0.1. The compliance of random ultimate strength values with the uniform distribution law is proved according to the Pearson's criterion. For each value of α, five various sets of FE strength properties are generated.

The solution algorithm of the problem (1)–(4) with the boundary conditions (6) is implemented in the Ansys Parametric Design Language (APDL). The FE destruction is carried out using the ANSYS built-in procedure "death of finite element", leading to the rigidity properties decrease by 10^6 times. The PLANE182 element with the linear displacements field approximation is used, the mesh is generated automatically. Solving the convergence problem (concentrator depth h=8 mm) demonstrated that it is sufficient to use the FE with the characteristic linear size of L_{el} =0.167 mm (defined as the square root of the ratio of the body area to the number of FE), which corresponds to the number of elements N=70994 (if h=4 mm, N=74166). The critical value of external load P_{crit} is selected equal to 1 kN to prevent the extreme increase in displacement u_0 if the α parameter value is large.

The results of the fracture process modeling are presented below.

RESULTS AND DISCUSSION

Regularities of the body damaging process without distribution in the FE strength properties

We consider the damage process of the elastic-brittle body with stress concentrator (h=8 mm) in case of equal FE ultimate strength values (α=0). Fig. 3 illustrates the loading diagram and the first principal stress σ_1 fields at the body's steady states 1–5. Several features can be noted. Primarily, first finite element destruction does not lead to macro-fracture of the entire body, the maximum load value increases by the ≈22%. Secondly, several load decline stages appear on the diagram. It is connected with crack propagation under constant boundary conditions down to getting stable state. Such sharp load drops (which do not lead to macro-fracture) are also observed in the real experimental diagrams of the elastic-brittle bodies. Thirdly, following the maximum load value reaching there are several steady states with lower external load. It indicates postcritical deformation stage realization for the solid with stress concentrator. The width of propagated crack is 1-2 finite elements, which is sufficient for accurate cracks description arising in elastic-brittle bodies during destruction. According to these findings, there is qualitative agreement of the damaging process modeling results with real experiments in terms of load-displacement diagrams [50-52] and macrodefect view [50, 53-56]. The α parameter value influence on the regularities of the damaging process is considered below.

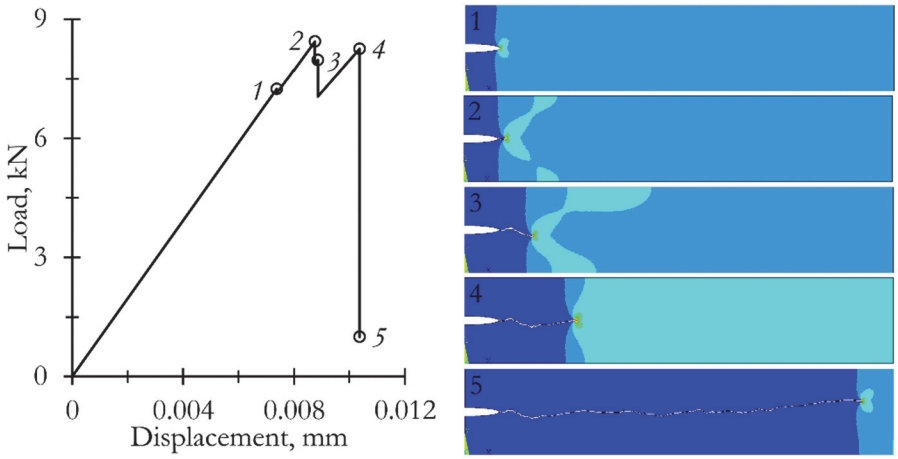

Figure 3: The calculated loading diagram (a) and the macrodefect growth kinetics (b) for the solid with α=0

Finite elements strength distribution range influence on the fracture process

Typical calculated loading diagrams for various parameter α value are presented in the Fig. 4a. The growth of α parameter provides the maximum load value increase, followed by the drop in load bearing capacity after reaching α=0.6. In this case, the displacement in the point of maximum value load shifts to the right, and then to the left, accordingly. The ultimate strength distribution range exert significant influence on the loading diagram shape. For example, at α≤0.3 postcritical deformation stage does not occur in all cases, the maximum load value getting is followed by its nonequilibrium decline. Small stages of the postcritical deformation are observed at 0.4≤α≤0.7, but the nonequilibrium stages are still extended. At 0.8≤α≤0.9 the loading diagram is relatively smooth, the long stages of sharp load drop do not practically exist, the extended softening stage is realized at macro-level accompanied by the increase of displacement value where damaging process modeling stops. Such load-displacement diagrams correspond to the brittle-ductile transition behavior, observed in quasi-brittle materials [57]. For a more detailed crack propagation consideration, the parameter ω is introduced, defining the relative number of destroyed elements as follows:

$$\omega = \frac{N_{destr}}{N} \tag{8}$$

where N_{destr} – destroyed elements number, N – total number of elements in the computational domain). Graphs of the parameter ω dependence on the body boundary displacement are shown in Fig. 4b. Symbol * marks the α values for which the graphs are plotted along the additional ordinate axis ω*. For small α the obtained curves are stepped, the maximum

arrival value is about 0.006, which corresponds to the macro-crack growth of 1-2 FE thick. For the large values of α, a much smoother, almost linear increase in ω is noted.

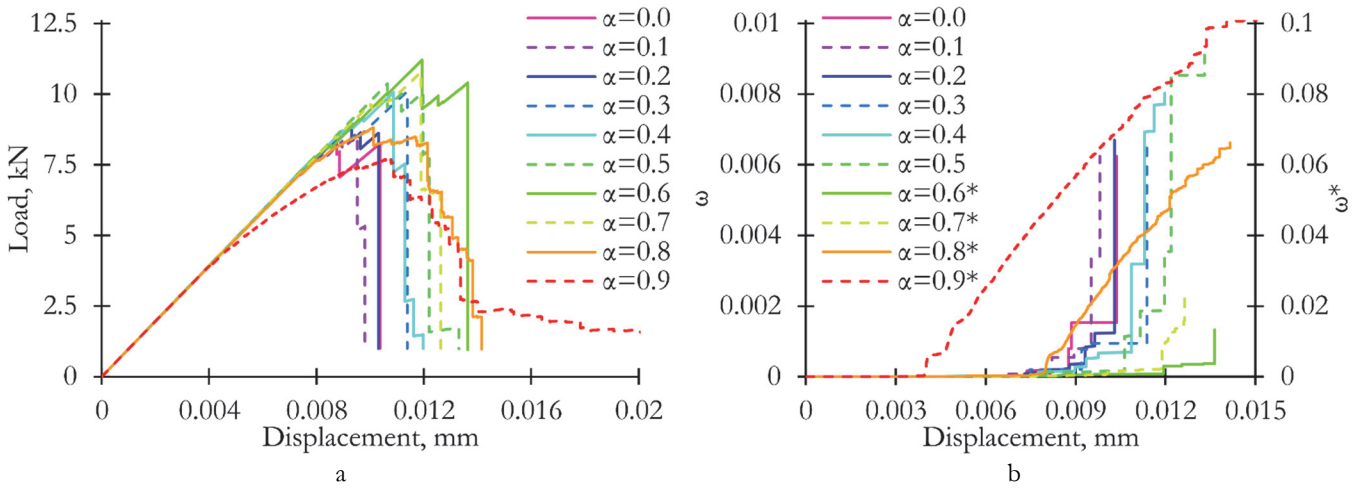

Figure 4: The calculated loading diagrams (a) and the corresponding increase in the relative number of destroyed elements (b) for the various values of α

Maximum load and ω parameter dependences on the α parameter are shown in the Fig. 5. Points on the graphs correspond to the average values over five computational simulations, the lines represent the deviations of these values from the average determined with standard methods. The maximum load bearing capacity value dependence on α illustrates that as the α increases, the load bearing capacity slowly grows, at the α=0.6 the maximum is reached (which also corresponds to brittle-ductile transition behavior [58]), then the sharp decline occurs, accompanied by the decrease in the deviation values. Therefore, small deviations in the strength properties lead to an increase in load bearing capacity, probably due to a change in the trajectory of the macrodefect and the presence of «strong» elements that interrupt its development. Large values of α, by contrast, decrease the load bearing capacity due to the presence of «weak» elements, through which a macrodefect subsequently proceeds. The graph of the ω(α) dependence monotonically increases, but changes slightly and has minor deviations until reaching α=0.5. At the large α values, the sharp increase in the number of destroyed finite elements is observed, which occurs due to the destruction of FE far from the concentrator area with increased stress values.

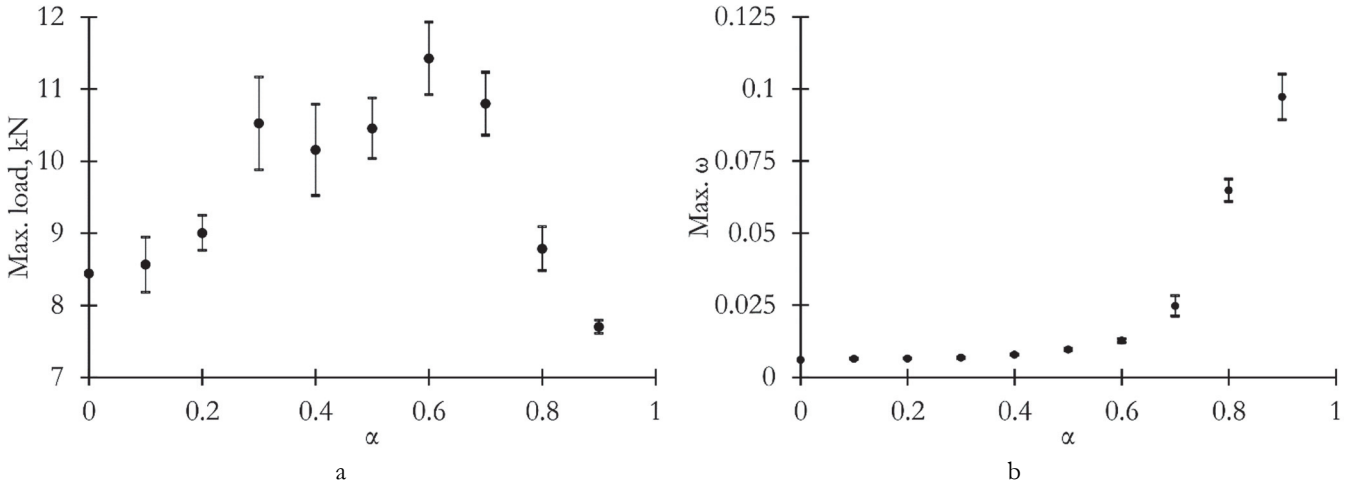

Figure 5: The dependencies of the maximum load value (a) and the maximum ω value (b) on α

To illustrate the various damage accumulation processes, the body states under the equal parameter ω=0.006 are considered. The images are given in Fig. 6 (as first principal stress fields). Results demonstrate that if α≤0.4, the macro-defect forms in the shape of main crack, however, the distance from the top of the concentrator to the last destroyed element gradually decreases. It happens due to the presence of several small branches, formed by the «weak» elements' destruction on the way

of the crack growth. In all the cases, the macro-defect develops approximately across the loading direction. At the α value of 0.5 and 0.6 a number of elements are destroyed close to the macro-defect without being connected with it, and the crack trajectory deviates from the straight. For the α=0.7 separate areas with destroyed FE are noted far from the concentrator. Consequently, the strength values range growth leads to the decrease in the stress concentration influence on the fracture process. At the α value of 0.8 and 0.9 elements are destroyed chaotically through the entire body. Moreover, at α=0.8 the formation of groups consisting of 2-3 destroyed FE is typical as compared to the groups from 1 FE if α=0.9. Thus, it can be concluded that parameter α has a significant influence on the evolution of the body damaging process. Several characteristic mechanisms of damage accumulation can also be noted: the growth of the macro-defect from the stress concentrator; the destruction of FE near the macro-defect in the region of stress concentration; the FE destruction far from the area of stress concentration.

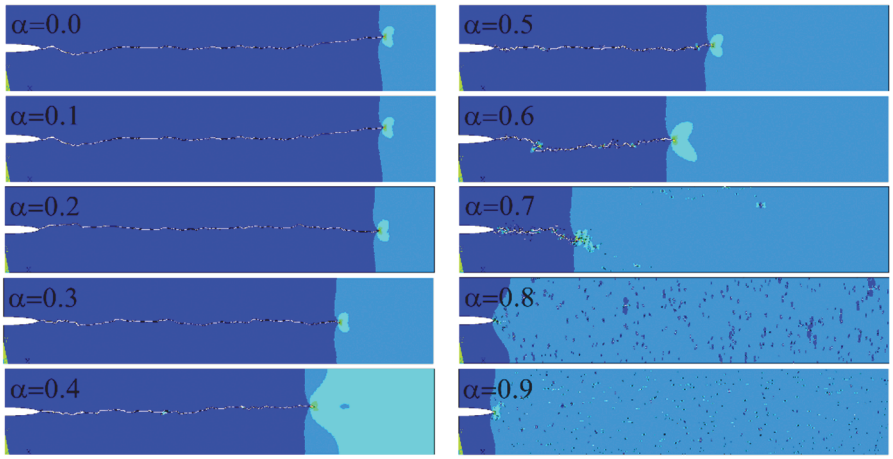

Figure 6: The images of bodies with various α at ω=0.006

For more detailed understanding of the damage accumulation mechanisms and their connection with loading diagrams the evolution of the damaged structure for the body with α=0.8 is considered. Fig. 7 represents the loading diagram and body images (first principal stress fields) corresponding to the certain states. After the elastic stage, destruction of individual FE is observed in the area fairly close to the stress concentrator (state 1). Until the maximum load value reaching, the damages cumulate throughout the entire body; occasionally combining into larger groups (states 2-3). Load decrease at the postcritical deformation stage is accompanied by the macro-defects development near the concentrator and in the middle part of the solid (states 4-5). The appearance of a main crack gradually begins to arise, further leading to separation of the body (states 6-8). At the same time, the destruction of separated FE not associated with macro-defects continues. After state 8, the load drop slows down, defects develop at an almost constant level of load, and a gradual closure of macro-defects formed in different parts of the body occurs (states 9-10). It is necessary to notice that, in the areas above and below of the concentrator, where the stresses are significantly lower, almost no damages occurred.

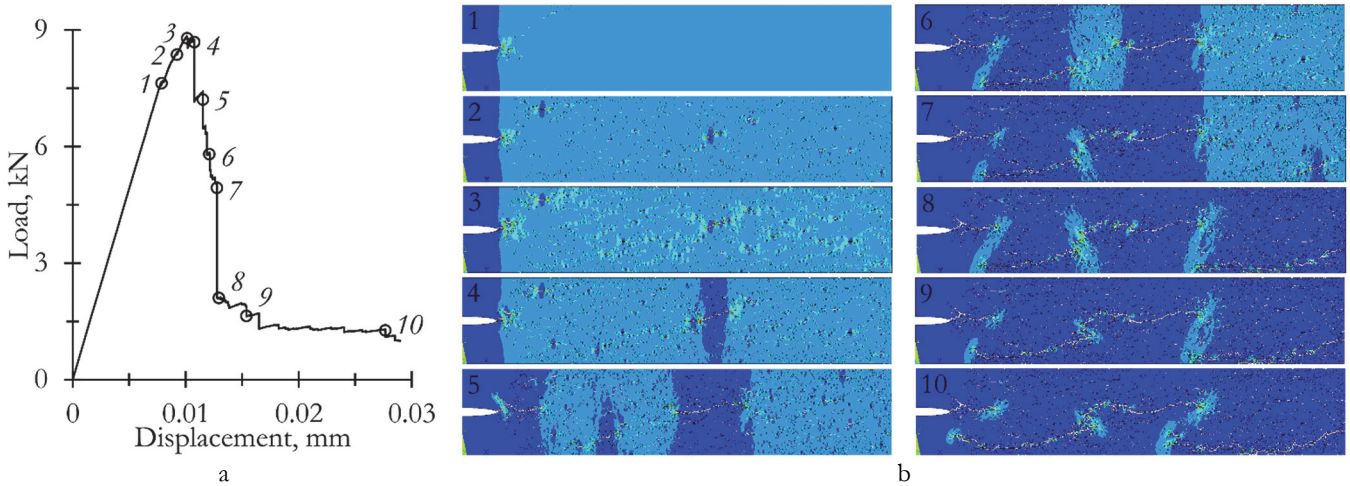

Figure 7: The calculated loading diagram (a) and the damages development kinetics (b) for the solid with α=0.8

Stress concentration value influence on the damaging process

Similar set of problems is solved for the body with h=4 mm (stress concentration, defined as the ratio of the normal stress σ_{yy} at the top of the concentrator and away from it is equal to 9.33 for h=8 mm and 7.06 for h=4 mm) in order to investigate stress concentration value influence on the damaging process. Typical calculated loading diagrams for various α parameter values are presented in the Fig. 8a. As well as for the body with h=8 mm, the nonmonotonic load bearing capacity dependence on α and qualitative change in the shape of loading diagrams are noted. The most significant difference between two concentrators is the greater implementation of the postcritical deformation stage. At h=8 mm sufficiently extended postcritical deformation stage begins to form for α≥0.4, in comparison with α=0.2 at h=4 mm. The obtained results correlate with the ω growth parameter curves presented in Fig. 8b. For the equal α values, the decrease in stress concentration leads to more equilibrium damage accumulation processes and greater number of stable states implementation.

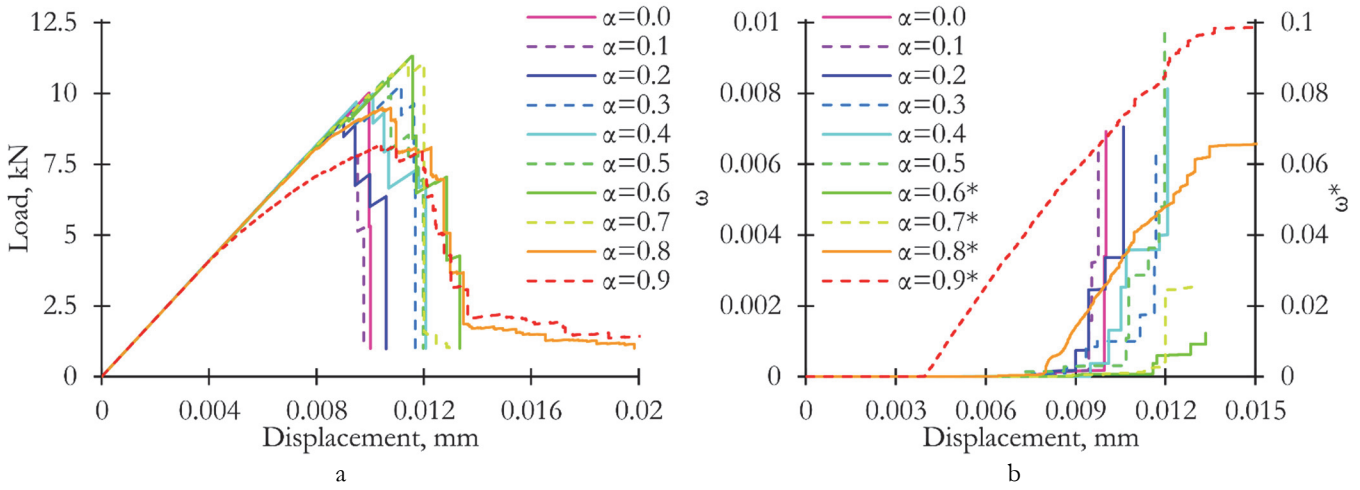

Figure 8: The calculated loading diagrams (a) and the corresponding increase in the relative number of destroyed elements (b) for the various values of α for the body with the stress concentrator depth of 4 mm

Stress concentration decrease leads to the change in maximum load and ω values dependencies on α, presented in the Fig. 9a, b. Firstly, concertation decrease causes the maximum loadability growth, however, this is also associated with the increase in cross-sectional area. Secondly, at h=8 mm maximum load value steadily grows, reaches maximum at α=0.6 and then falls, while at h=4 mm in the range of 0≤α≤0.4 the load bearing capacity changes slightly, even get lower, whereafter increase, reaching maximum value at to α=0.6 and then falls. At the higher stress concentration, the maximum load at α=0.9 is 8.7% lower than at α=0.0, while decrease in the stress concentration changes this value by 19.3%, and deviations from the average grow. The insignificant change in ω(α) dependence is also noted; only a slight increase in the maximum value of ω occurs. A comparison is made between the average values of the conditional maximum stress values, defined as the ratio of the maximum load to the narrowest cross-sectional area (Fig. 9c). Up to the value of α=0.5 the maximum conditional stress differs significantly, but then the graphs are extremely close. We assume the existence of critical α parameter values, upon reaching which the stress concentration ceases to influence the damaging process and bearing capacity. It is necessary to confirm this hypothesis in future studies.

The stress concentration influence on the damaged structure under similar values of ω equal to 0.006 is considered and illustrated in the Fig. 10 as the first principal stress fields. The decrease in stress concentration leads to the non-monotonic dependence of macro-defect length on α. In addition, a more significant macro-defect trajectory deviation from the straight line is observed. Significant differences are noted for the value α=0.7, at which separated defects groups in the body and two growing macro-defects are observed: from the concentrator and from the opposite side of the body. Consequently, stress concentration reduction causes increase in probability of macro-defect development outside of the concentrator area. Otherwise, the obtained results correspond to those for the higher stress concentration. The damage accumulation typical mechanisms remain unchanged, as do the parameter α values ranges at which they appear.

The damaged structure evolution at α=0.8 is analyzed, the loading diagram and body images (first principal stress fields) corresponding to several states are shown in Fig. 11. For the h=8 mm the fusion of separated destroyed FE into macro-defects begin to appear before the maximum load value is achieved, while the decrease in stress concentration leads to the macro-defects formation at the postcritical deformation stage, which is more extended at the initial stage. For the states 3-8, a less sharp drop in the load is observed than for a higher stress concentration. Nevertheless, the mechanism of macro-

defect propagation practically does not change. The deviation of the macro-defect from a straight line reduces. Thus, the stress concentration value affects the damage accumulation process. It seems appropriate to conduct further studies with the extended range of stress concentration value.

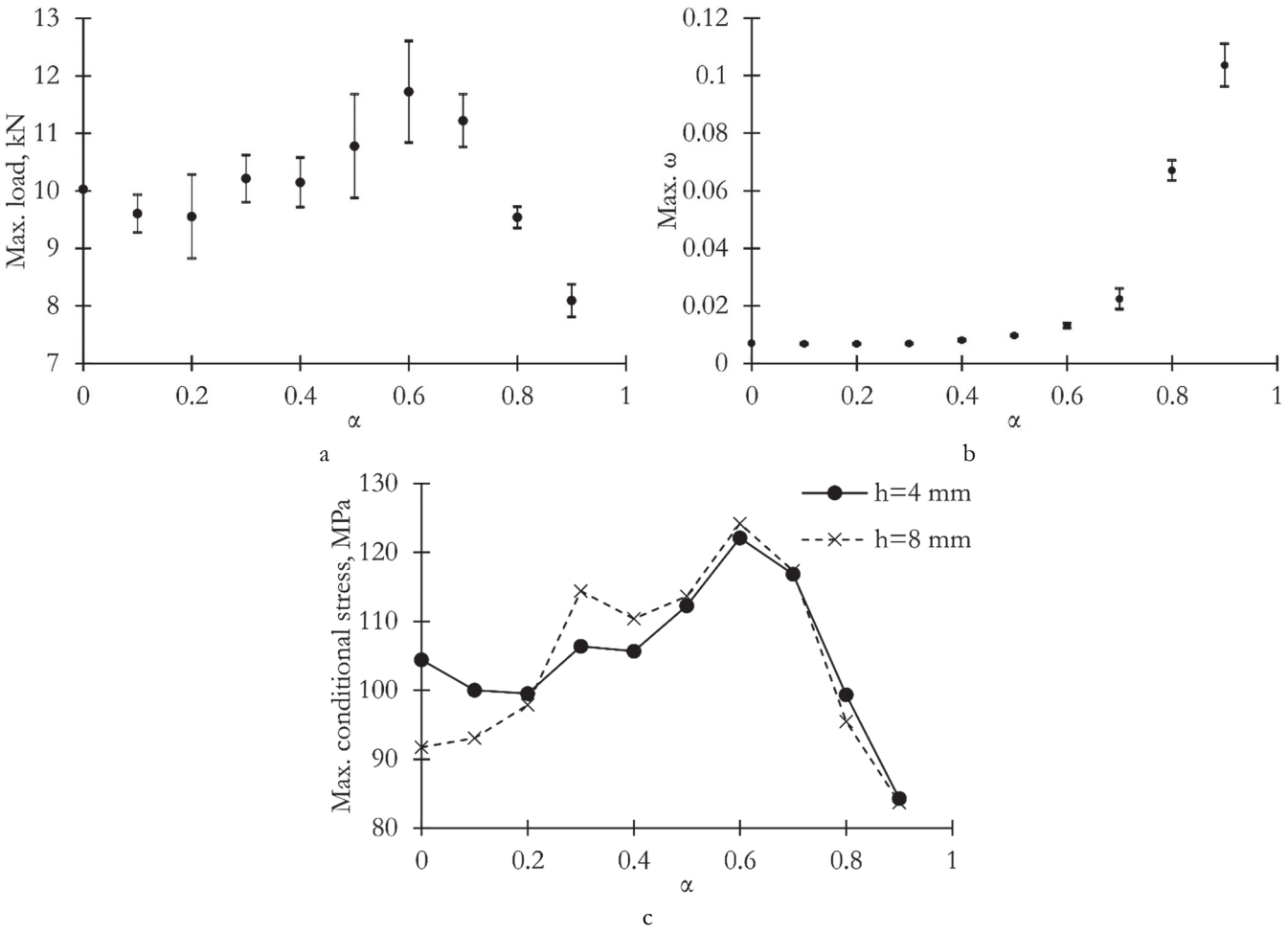

Figure 9: The dependencies of the maximum load value (a) and the maximum ω value (b) on α for the body with the stress concentrator depth of 4 mm; comparison between maximum conditional stress average values for the bodies with different *h* (c)

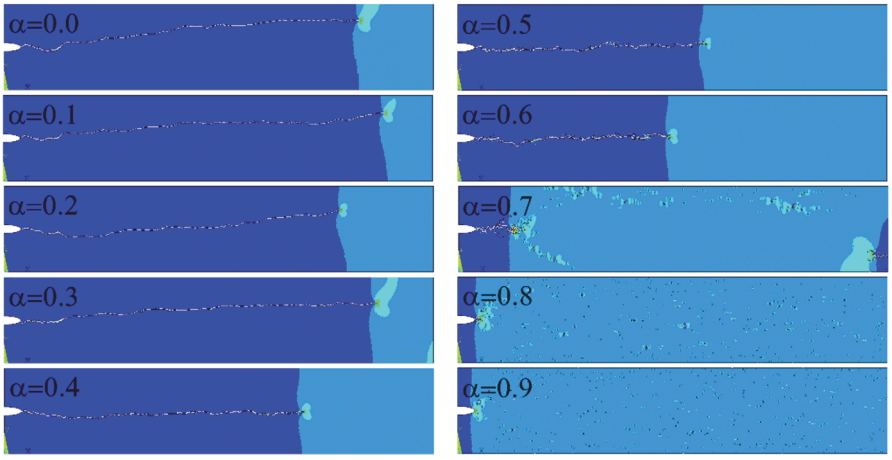

Figure 10: The images of bodies with various α at ω=0.006 for the body with the stress concentrator depth of 4 mm

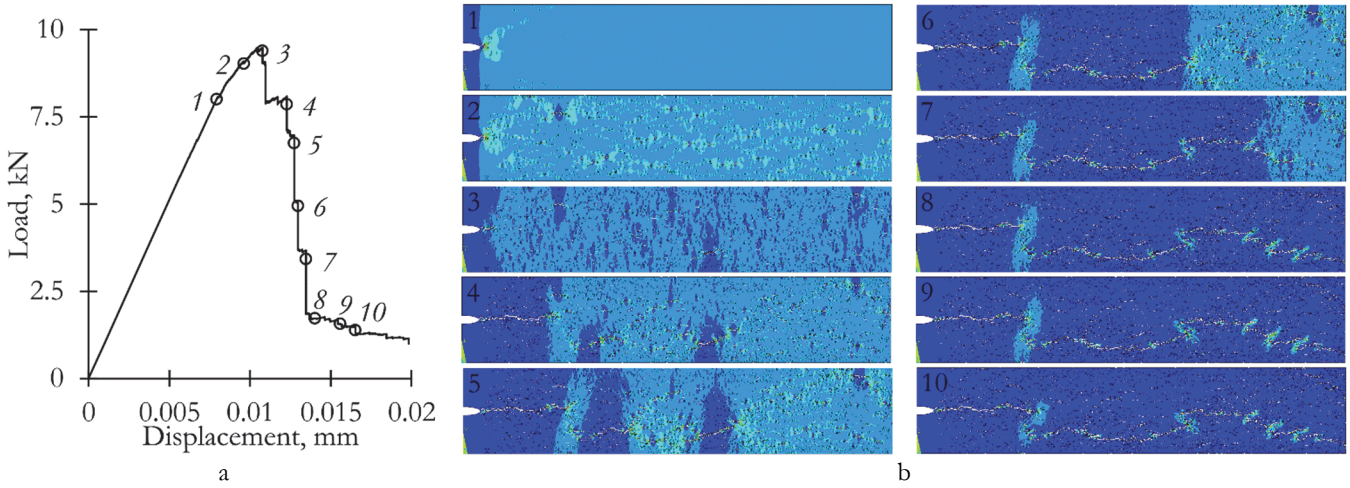

Figure 11: The calculated loading diagram (a) and the damages development kinetics (b) for the solid with α=0.8 for the body with the stress concentrator depth of 4 mm

Mesh sensitivity analysis

Since the size of the FE may significantly influence the damaging process modeling results, the mesh sensitivity analysis is performed on the problem of the kinematic loading of the plate with the stress concentrator (h=8 mm) without the FE strength properties distribution (α=0.0). The automatically generated meshes with the characteristic linear size L_{el} (defined as the square root of the ratio of the body area to the number of FE) of 0.167, 0.143, 0.121, 0.097 and 0.073 mm (corresponding to the number of elements N=70994, 97252, 136573, 209723 and 383781) are used. Fig. 12 represents the calculated loading diagrams and corresponding graphs of increase in the relative number of destroyed elements. The absence of the results' convergence is noted. The FE size decrease leads to the maximum load and maximum ω values reduction, although the damages development kinetics and mechanism of macro-defect propagation are changed slightly. By comparing experimental data on the deformation of elastic-brittle bodies with the results of damaging process numerical modeling obtained using various meshes, the rational size of the FE can be defined, reflecting the typical size of the single act of destruction [37]. Based on the above, the mesh sensitivity has to be taken into account while modeling the damaging process of elastic-brittle solids with statistically distributed strength properties over the body volume.

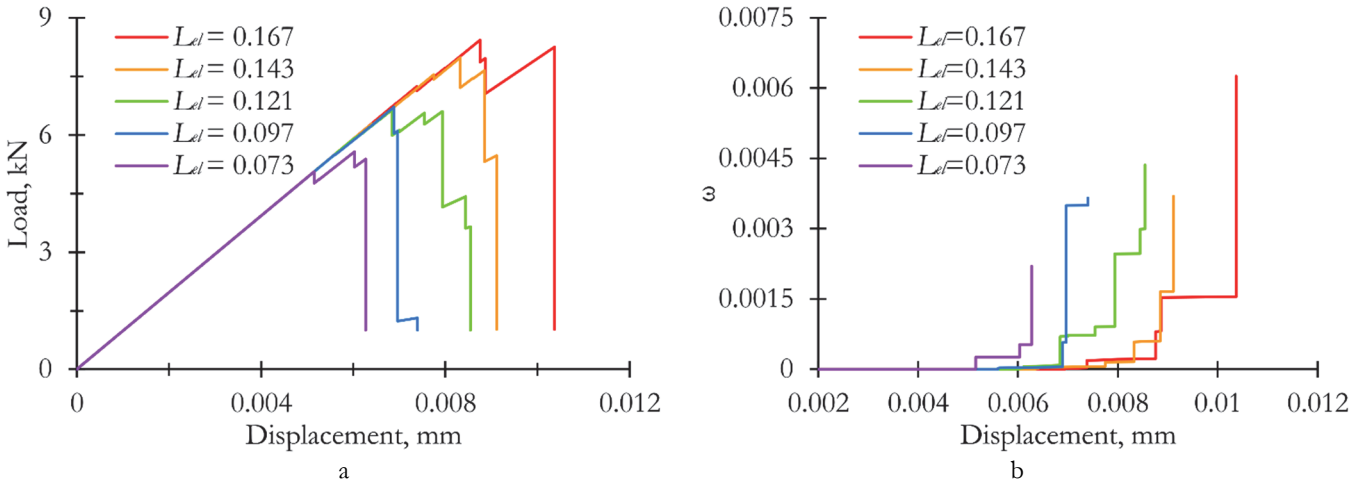

Figure 12: The calculated loading diagrams (a) and the corresponding increase in the relative number of destroyed elements (b) for the various values of characteristic linear size L_{el}

CONCLUSIONS

This paper is devoted to the problem of fracture processes numerical modeling of elastic-brittle bodies with stress concentrators taking into account the structural elements strength properties distribution. The main results of the study are:

- The novel boundary value problem formulation has been proposed. Its advantages and disadvantages have been noted. The solving algorithm has been developed and implemented in APDL.
- The regularities of fracture process have been analyzed in the case of ultimate strength distribution absence. The fracture process consideration has allowed to identify the additional load bearing capacity. The postcritical deformation stage implementation has been noted.
- The influence of the ultimate strength distribution range (characterized by the parameter α) on the maximum load value, loading curve shape and damage accumulation processes has been studied. The maximum load value depends nonmonotonically on α, the maximum is achieved at α=0.6. The distribution range increase leads to significant growth in the number of destructed elements. The basic mechanisms of damage accumulation are: elements destruction in the stress concentration area leading to macro-defect growth; elements fracture close to the macro-defect; elements destruction far from the concentrator.
- The stress concentration value influence on the fracture process has been investigated. The concentrator's depth decrease leads to the significant change in the damage accumulation kinetics and maximum load dependence on α parameter.
- The mesh sensitivity analysis has been carried out. The FE size decrease leads to the maximum load and maximum relative number of destroyed elements values reduction without changing the damaging process kinetics.
- The hypothesis has been put forward on existence of critical α parameter value, upon reaching which the stress concentrator stops having the influence on the body's fracture process.

The further investigation will be dedicated to the stated hypothesis confirmation, taking into account the finite elements size and statistical distribution type.

ACKNOWLEDGEMENTS

The work was carried out with support of the Russian Science Foundation (Project № 22-19-00765, https://rscf.ru/project/22-19-00765/) in the Perm National Research Polytechnic University.

REFERENCES

[1] Bažant, Z.P. (1976). Instability, ductility, and size effect in strain-softening concrete, J. Eng. Mech. Div., 102 (2), pp. 331-344.

[2] Bažant, Z.P. and Di Luzio, G. (2004). Nonlocal microplane model with strain-softening yield limits, International Journal of Solids and Structures, 41 (24-25), pp. 7209-7240. DOI:10.1016/j.ijsolstr.2004.05.065.

[3] Boyce, B.L., Kramer, S.L.B., Fang, H.E. (2014). The Sandia Fracture Challenge: blind round robin predictions of ductile tearing, International Journal of Fracture, 186, pp. 5-68. DOI: 10.1007/s10704-013-9904-6.

[4] Galavi, V. and Schweiger, H.F. (2010). Nonlocal multilaminate model for strain softening analysis, International Journal of Geomechanics, 10(1), pp. 30-44. DOI: 10.1061/(ASCE)1532-3641(2010)10:1(30).

[5] Tashkinov, M., Ershova, D., and Shalimov, A. (2019). Computational multi-scale analysis of simultaneous processes of delamination and damage accumulation in laminated composites, Frattura ed Integrità Strutturale, 49, pp.396-411. DOI: 10.3221/IGF-ESIS.49.39.

[6] Xiao, D., Yang, W., Liu, C., and Hu, R. (2022). Testing of Mode-I Fracture Toughness of Sandstone Based on the Fracturing Mechanism of an Explosion Stress Wave, Rock Mechanics and Rock Engineering, 55, pp. 7731–7745, DOI: 10.1007/s00603-022-03047-8.

[7] Yarullin, R.R., Shlyannikov, V.N, Ishtyriakov, I.S. and Yakovlev M.M. (2020). Stress intensity factors for mixed-mode crack growth in imitation models under biaxial loading, Frattura ed Integrità Strutturale, 53, pp. 210-222. DOI: 10.3221/IGF-ESIS.53.18.

[8] Zhang, X.-Q., Zhang, X., Li, L., Duan, S.-W., Li, S.-Z., Huang, Z.-L., Zhang Y.-W., and Feng, J.-Y. (2016). Investigation of the Influence of Small Hole on the Fatigue Crack Growth Path, Journal of Failure Analysis and Prevention, 16, pp.391–399. DOI: 10.1007/s11668-016-0098-x.
[9] Sukumar, N., Dolbow, J.E. and Moës, N. (2015). Extended finite element method in computational fracture mechanics: a retrospective examination, International Journal of Fracture, 196, pp. 189-206. DOI: 10.1007/s10704-015-0064-8
[10] Wang, F., Wei, Z., Li, P., Yu, L. and Huang, W. (2019). Initial Crack Propagation and the Influence Factors of Aircraft Pipe Pressure, Materials (Basel), 12(19), 3098. DOI: 10.3390/ma12193098.
[11] Benvenutia, E., Chiozzia, A., Manzinib, G. and Sukumarc, N. (2021), Extended virtual element method for the Laplace problem with singularities and discontinuities, Comput. Methods in Appl. Mech. Engrg., 356, pp. 571-597. DOI: 10.1016/j.cma.2019.07.028.
[12] Marfia, S., Monaldo, E. and Sacco, E. (2022), Cohesive fracture evolution within virtual element method, Engineering Fracture Mechanics, 269, 108464. DOI: 10.1016/j.engfracmech.2022.108464.
[13] Ongaro, G., Bertani, R., Galvanetto, U., Pontefisso, A. and Zaccariotto, M. (2022), A multiscale peridynamic framework for modelling mechanical properties of polymer-based nanocomposites, Engineering Fracture Mechanics, 274, 108751. DOI: 10.1016/j.engfracmech.2022.108751.
[14] Xu, W., Tong, Z., Rong, D., Leung, A.Y.T., Xu, X., and Zhou, Z. (2017). Determination of stress intensity factors for finite cracked bimaterial plates in bending, Archive of Applied Mechanics 87, pp. 1151–1163. DOI:10.1007/s00419-017-1239-8.
[15] Rabczuk, T., Bordas, S. and Zi, G. (2010). On three-dimensional modelling of crack growth using partition of unity methods, Computers & Structures, 88 (23-24), pp. 1391-1411. DOI:10.1016/j.compstruc.2008.08.010.
[16] De-Pouplana, I. and Oñate, E. (2016). Combination of a non-local damage model for quasi-brittle materials with a mesh-adaptive finite element technique, Finite Elements in Analysis and Design, 112, pp. 26-39. DOI: 10.1016/j.finel.2015.12.011.
[17] Kumchol, Y., Zhenqing, W., Mengzhou, C., Jingbiao, L., Tae-Jong, K., Namjin, S., Kyongsu, J. and Sakaya, R. (2019). A computational methodology for simulating quasi-brittle fracture problems, Computers & Structures, 215, pp. 65-79. DOI: 10.1016/j.compstruc.2019.02.003
[18] Wildemann, V.E. and Mugatarov, A.I. (2022). Modeling the process of equilibrium crack growth in a composite specimen from the standpoints of the postcritical deformation mechanics, J. Samara State Tech. Univ., Ser. Phys. Math. Sci., 1, pp. 48–61. DOI: 10.14498/vsgtu1886
[19] De Maio, U., Gaetano, D., Greco, F., Lonetti, P. and Pranno, A. (2023), The damage effect on the dynamic characteristics of FRP-strengthened reinforced concrete structures, Composite Structures, 309, 116731. DOI:10.1016/j.compstruct.2023.116731.
[20] De Maio, U., Gaetano, D., Greco, F., Lonetti, P., Blasi, P.N. and Pranno, A. (2023), The Reinforcing Effect of Nano-Modified Epoxy Resin on the Failure Behavior of FRP-Plated RC Structures, High-Performance Reinforced Concrete Structures and Composites, 13(5), 1139. DOI: 10.3390/buildings13051139.
[21] Carpinteri, A. and Accornero, F. (2019), The Bridged Crack Model with multiple fibers: Local instabilities, scale effects, plastic shake-down, and hysteresis, Theoretical and Applied Fracture Mechanics, 104, 102351. DOI: 10.1016/j.tafmec.2019.102351.
[22] Dezfuli, F.H. and Alam, M.S. (2014) Sensitivity analysis of carbon fiber reinforced elastomeric isolators based on experimental tests and finite element simulations, Bull Earthquake Eng, 12, pp. 1025-1043. DOI:10.1007/s10518-013-9556-y.
[23] Feklistova, E.V., Tretyakov, M.P. and Wildemann, V.E. (2021). Numerical implementation issues of the deformation and destruction process of bodies with stress concentrators. AIP Conference Proceedings, 2371(1), 050002. DOI: 10.1063/5.0059553.
[24] Nicoletto, G. and Riva, E. (2004). Failure mechanisms in twill-weave laminates: FEM predictions vs. experiments, Composites Part A: Applied Science and Manufacturing, 35 (7–8), pp. 787-795. DOI: 10.1016/j.compositesa.2004.01.007.
[25] Zhao, L.G., Warrior, N.A., and A.C. Long, (2006). Finite element modelling of damage progression in non-crimp fabric reinforced composites, Composites Science and Technology, 66 (1), pp. 36-50. DOI: 10.1016/j.compscitech.2005.06.002.
[26] Feklistova, E.V., Tretyakov, M.P. and Wildemann, V.E. (2019). Studying the influence of numerical simulation parameters on the solutions of boundary value problems on the destruction of bodies with crack-like defects, IOP Conference Series Materials Science and Engineering, 747(1), 012110. DOI:10.1088/1757-899X/747/1/012110.

[27] Kasparova, E.A. and Shushpannikov, P.S. (2018). Numerical and analytical methods for simulation of growth and interaction of crack, Computational Continuum Mechanics, 11(1), pp. 79-91. DOI:10.7242/1999-6691/2018.11.1.7
[28] Smetannikov, O.Y., Kashnikov, Y.A., Ashihmin, S.G. and Shustov, D.V. (2015). Numerical model of crack growth in hydraulic re-fracturing, Computational Continuum Mechanics, 8(2), pp. 208-218. DOI: 10.7242/1999-6691/2015.8.2.18
[29] Ilinykh, A.V. and Vildeman, V.E. (2012). Modeling of structure and failure processes of granular composites, Computational Continuum Mechanics, 5(4), pp. 443-451. DOI:10.7242/1999-6691/2012.5.4.52.
[30] Novoselov, A.V. and Vildeman, V.E. (2012). Structural failure behavior research for the planar stressed plates based on numerical modeling, Perm National Research Polytechnic University Mechanics Bulletin, 4, pp. 66-78.
[31] Wildemann, V.E. and Ilynykh, A.V. (2007). Simulation of structural failure and scale effects of softening at the post-critical deformation stage in heterogeneous media, Physical Mesomechanics, 10(4), pp. 23-29.
[32] Ahmad, M., Ismailb, K..A., and Mata, F., Convergence of Finite Element Model for Crushing of a Conical Thin- walled Tube, Procedia Engineering, 53, pp. 586 – 593. DOI: 10.1016/j.proeng.2013.02.075.
[33] Kõrgesaar, M. and Romanoff, J. (2014). Influence of mesh size, stress triaxiality and damage induced softening on ductile fracture of large-scale shell structures, Marine Structures, 38, pp. 1-17. DOI: 10.1016/j.marstruc.2014.05.001.
[34] Lopes, B., Arruda, M.R.T. and Almeida-Fernandes, L. et al. (2020) Assessment of mesh dependency in the numerical simulation of compact tension tests for orthotropic materials, Composites Part C: Open Access, 1, 100006. DOI: 10.1016/j.jcomc.2020.100006.
[35] Monforte, L., Ciantia, M.O., Carbonell, J.M. et al. (2019). A stable mesh-independent approach for numerical modelling of structured soils at large strains, Computers and Geotechnics, 116, 103215. DOI:10.1016/j.compgeo.2019.103215
[36] Sanjaya, Y., Prabowo, A.R., Imaduddin, F. and Nordin, N.A., B. (2021). Design and Analysis of Mesh Size Subjected to Wheel Rim Convergence Using Finite Element Method, Procedia Structural Integrity, 33, pp. 51-58. DOI: 10.1016/j.prostr.2021.10.008.
[37] Wildemann, V.E., Feklistova, E.V., Mugatarov, A.I., Mullahmetov, M.N., and Kuchukov, A.M. (2023). Aspects of numerical simulation of failure of elastic-brittle solids, Computational Continuum Mechanics, 16 (4), pp. 420-429. DOI: 10.7242/1999-6691/2023.16.4.35.
[38] Chen, X. and Li J. (2023). An extended two-scale random field model for stochastic response analysis and its application to RC Short-leg shear wall structure, Probabilistic Engineering Mechanics, 74, 103508. DOI:10.1016/j.probengmech.2023.103508.
[39] Chmel, A. and Shcherbakov, I. (2014). Damage initiation in brittle and ductile materials as revealed from a fractoluminescence study, Frattura ed Integrità Strutturale, 30, pp. 162-166. DOI: 10.3221/IGF-ESIS.30.21.
[40] Hai, L. and Lyu M.-Z. (2023). Modeling tensile failure of concrete considering multivariate correlated random fields of material parameters, Probabilistic Engineering Mechanics, 74, 103529. DOI: 10.1016/j.probengmech.2023.103529.
[41] Lobanov, D.S., Yankin, A.S. and Berdnikova N.I. (2022). Statistical evaluation of the effect of hygrothermal aging on the interlaminar shear of GFRP, Frattura ed Integrità Strutturale, 60, pp. 146-157; DOI: 10.3221/IGF-ESIS.60.11.
[42] Lobanov, D.S., Lunegova, E.M. and Mugatarov A.I. (2021). Influence of preliminary thermal aging on the residual interlayer strength and staging of damage accumulation in structural carbon plastic, PNRPU Mechanics Bulletin, 1, pp. 41-51. DOI: 10.15593/perm.mech/2021.1.05.
[43] Peng, Z., Wang, X. and Wu, Z. (2020). Multiscale strength prediction of fiber-reinforced polymer cables based on random strength distribution, Composites Science and Technology, 196, 108228. DOI:10.1016/j.compscitech.2020.108228
[44] Zweben, C. and Rosen, B.W. (1970). A statistical theory of material strength with application to composite materials, Journal of the Mechanics and Physics of Solids, 18(3), pp. 189-206. DOI: 10.1016/0022-5096(70)90023-2.
[45] Belaïd, M., Malika, M., Mokadem, S., and Boualem S. (2020). Probabilistic elastic-plastic fracture mechanics analysis of propagation of cracks in pipes under internal pressure, Frattura ed Integrità Strutturale, 54, pp. 202-210. DOI: 10.3221/IGF-ESIS.54.15.
[46] Mishnaevsky, L.Jr. and Brøndsted, P. (2009). Micromechanisms of damage in unidirectional fiber reinforced composites: 3D computational analysis, Composites Science and Technology, 69 (7-8), pp. 1036-1044. DOI:10.1016/j.compscitech.2009.01.022.
[47] Bažant, Z.P. (1999), Size effect on structural strength: a review, Archive of Applied Mechanics, 69, pp. 703-725.
[48] Ramamurty, U., McNulty, J.C., Steen, M. and Li, L.B. (2000). Fatigue in Ceramic Matrix Composites, Comprehensive Composite Materials, 4, pp 163-219. DOI: 10.1016/B0-08-042993-9/00093-0
[49] Zheng, T., Guo, L., Ding, J. and Li, Z. (2022). An innovative micromechanics-based multiscale damage model of 3D woven composites incorporating probabilistic fiber strength distribution, Composite Structures, 287, 115345.

DOI: 10.1016/j.compstruct.2022.115345.
[50] Cao, Ri-H., Cao, P., Lin, H., Pu C.-Z. and Ou, K. (2016). Mechanical Behavior of Brittle Rock-Like Specimens with Pre-existing Fissures Under Uniaxial Loading: Experimental Studies and Particle Mechanics Approach, 49, pp. 763–783. DOI:10.1007/s00603-015-0779-x
[51] Zheng, T., Guo, L., Ding, J. and Li, Z. (2022). An innovative micromechanics-based multiscale damage model of 3D woven composites incorporating probabilistic fiber strength distribution, Composite Structures, 287, 115345. DOI: 10.1016/j.compstruct.2022.115345.
[52] Chen, X. and Li, J. (2023). An extended two-scale random field model for stochastic response analysis and its application to RC Short-leg shear wall structure, Probabilistic Engineering Mechanics, 74, 103508. DOI: 10.1016/j.probengmech.2023.103508.
[53] Bui, T.Q., Tran, H.T., Hu, X. and Wu, C.-T. (2022). Simulation of dynamic brittle and quasi-brittle fracture: a revisited local damage approach, International Journal of Fracture, 236, pp. 59–85. DOI: 10.1007/s10704-022-00635-1.
[54] Chen, B., Yu, T., Natarajan, S., Zhang Q. and Bui, T. Q. (2023). Numerical simulation for quasi-static crack growth and dynamic crack branching by coupled state-based PD and XFEM, Acta Mechanica, 234, pp. 3605–3622. DOI: 10.1007/s00707-023-03585-4.
[55] Braun, M. and Fernández-Sáez, J. (2016). A 2D discrete model with a bilinear softening constitutive law applied to dynamic crack propagation problems, International Journal of Fracture, 197, pp. 81-97. DOI: 10.1007/s10704-015-0067-5.
[56] Fu, J., Haeri, H., Sarfarazi, V., Abharian, S., Jahanmiri, S. and Elahi, A. (2024). Investigations into size dependence on the behavior of rocks with a "V" notch and hole under uniaxial compression, Engineering Failure Analysis, 107960. DOI: 10.1016/j.engfailanal.2024.107960.
[57] Kosteski, L.E., Iturrioz, I., Friedrich, L.F. and Lacidogna, G. (2022). A study by the lattice discrete element method for exploring the fractal nature of scale effects, Scientific Reports, 12, 16744. DOI: 10.1016/0013-7944(85)90015-3.
[58] Carpinteri, A., Marega, C. and Savadori, A. (1985), Ductile-brittle transition by varying structural size, Engineering Fracture Mechanics, V.21(2), pp. 263-271. DOI: 10.1038/s41598-022-20137-3.